Journal Name

ARTICLE

High-Efficiency Bubbles Transportation in Aqueous Environment on Serial-Wedge-Shaped Wettability Pattern

Received 00th January 20xx,
Accepted 00th January 20xx

DOI: 10.1039/x0xx00000x

www.rsc.org/

Jinlong Song,[#a] Ziai Liu,[#a] Xuyue Wang,[a] Hong Liu,*[b] Yao Lu,[c] Xu Deng,[d] Claire J. Carmalt,[e] and Ivan P. Parkin[e]

Spontaneous and directional pumpless transportation (SDPT) of subaqueous gas bubbles has great prospects in eliminating the destructive gas bubbles in fluid transportation pipes. However, with current technology it is difficult to realize the non-buoyancy driven long-distance SDPT. How to realize the long-distance SDPT of subaqueous gas bubbles and how to fabricate the surface with the capacity of long-distance SDPT of subaqueous gas bubbles on engineering metal materials still remains a challenge. Here, a serial-wedge-shaped wettability pattern with the exterior surrounding subaqueous superaerophobic region and inside interior subaqueous superaerophilic region is designed to realize the long-distance SDPT of subaqueous gas bubbles. The process is driven by unbalanced surface tension forces, hence, subaqueous gas bubbles not only can be transported on the horizontal and straight pattern, but can also be easily transported on the horizontal and spiral-shaped pattern or on a wave-shaped pattern that is spatially tilted. In addition, a universal method composed of electrochemical etching and laser etching is also proposed to fabricate the serial-wedge-shaped wettability pattern on various engineering metal materials including Al, Mg alloy, Ti alloy, and Zn.

1 Introduction

Although superhydrophobic surfaces and superhydrophilic surfaces have been widely studied for more than 20 years,[1-6] they still fascinate more scientists because of their potential applications in the fields of self-cleaning,[1] anti-icing,[7] anti-corrosion,[8] oil/water separation,[9] drag-reduction,[10] and liquid transportation,[11] etc. In recent years, researchers have transferred their attentions to superhydrophobic surfaces and superhydrophilic surfaces under different fluids. They found that superhydrophobic surfaces show subaqueous superoelophilicity and can capture micron-sized oil droplets from water;[12,13] while superhydrophilic surfaces show subaqueous superoleophobicity and can resist organism-adhesion and crude-oil-adhesion.[14,15] On the basis of the aforementioned studies, researchers have recently found that subaqueous gas bubbles show similar behaviour as oil droplets on superhydrophobic surfaces and superhydrophilic surfaces, that is subaqueous superaerophilicity for superhydrophobic surfaces and subaqueous superaerophobicity for superhydrophilic surfaces.[16] New attention has been focused on the application of subaqueous superaerophobic surfaces and superaerophilic surfaces, which include collection and transportation of subaqueous gas bubbles and the ultrahigh evolution of subaqueous gas bubbles on electrodes.[17-24]

Subaqueous gas bubbles often exist in water, which may cause serious damage to the transportation system. For example, gas bubbles of carbon dioxide, hydrogen sulphide, and oxygen in the aqueous medium in pipelines often accelerate the hydrogenation and corrosion of inner metal walls, causing leakage and/or blockage of the fluid transportation pipes.[25, 26] Traditional methods to remove gas bubbles including chemical, ultrasonic, and thermal treatments; these have drawbacks due to the residue of the chemical reagents, the requirement of special equipment or high energy consumption. Environment and economy emphasize the use of more environment-friendly and energy efficient methods to eliminate subaqueous gas bubbles in the aqueous medium. Subaqueous superaerophobic surfaces and superaerophilic surfaces have been studied by researchers to realize the spontaneous and directional pumpless transportation (SDPT) of subaqueous gas bubbles. This can be used to collect and eliminate gas bubbles. Recent research focusing on the SDPT of subaqueous gas bubbles can be classified into two categories: one is buoyancy driven transportation[27-29] and the other is surface tension driven transportation based on shape-gradient surfaces.[30-33] Buoyancy driven transportation can only drive the gas bubbles upward. In comparison, surface tension

[a] Key Laboratory for Precision and Non-traditional Machining Technology of the Ministry of Education, Dalian University of Technology, Dalian 116024, P. R. China.
[b] Key Laboratory of Theoretical Chemistry of Environment Ministry of Education, South China Normal University, Guangzhou 510006, P. R. China. Email: hongliu@m.scnu.edu.cn
[c] Department of Mechanical Engineering, University College London, London, WC1E 7JE, UK.
[d] Institute of Fundamental and Frontier Sciences, University of Electronic Science and Technology of China, Chengdu 610054, P. R. China.
[e] Department of Chemistry, University College London, 20 Gordon Street, London, WC1H 0AJ, UK.
[#] Contribute equally

† Electronic Supplementary Information (ESI) available: [details of any supplementary information available should be included here]. See DOI: 10.1039/x0xx00000x

driven transportation based on the shape-gradient surfaces can drive gas bubbles upward, horizontally, and downward, hence exhibiting greater potential for application. The shape-gradient surfaces, including the 3D wettability cone and single-wedge-shaped wettability pattern, can realize the SDPT of subaqueous gas bubbles. In 2016, Yu et al. and Xue *et al*. found successively that the subaqueous superaerophilic Cu cone was capable of spontaneously and directionally transporting gas bubbles in an aqueous environment.[30,31] In 2018, Ma *et al*. fabricated a subaqueous superaerophilic polyethylene wedge which is the typical single-wedge-shaped wettability pattern and can realize the SDPT of subaqueous gas bubbles by using laser-cutting, sandpaper abrasion, and spraying superhydrophobic nanoparticles.[32] In the same year, Zhang *et al*. found that the subaqueous slippery wedge demonstrated a high adhesive force but low friction force with gas bubbles and could also realize the SDPT of subaqueous gas bubbles.[33] However, for the 3D wettability cone and single-wedge-shaped wettability pattern, gas bubbles are transported only from the narrow side to the wide side, indicating that the terminal size of the pattern for long-distance transportation will be large, which further means that the existing shape-gradient surfaces cannot be used for the long-distance transportation of subaqueous gas bubbles. How to realize the long-distance SDPT of subaqueous gas bubbles and how to fabricate the surface with the capacity of long-distance SDPT of subaqueous gas bubbles on engineering metal materials are key for many industrial challenges.

In this work, we developed a serial-wedge-shaped wettability pattern, which is composed of a front triangle and several rear trapezoids and connecting end to end, to successfully realize the long-distance SDPT of subaqueous gas bubbles. Differing from the conventional shape-gradient surfaces,[30-33] the terminal size of the serial-wedge-shaped wettability pattern has no relationship with the length of the whole pattern. When a gas bubble with a certain volume is transported, the transportation distance on the serial-wedge-shaped pattern will be much longer owing to its smaller superficial area. . The main driving force for gas bubbles on the serial-wedge-shaped wettability pattern is the unbalanced surface tension force originated from the Laplace pressure difference. The influence of the main parameters of the pattern on the transportation behavior was also systemically studied. For the serial-wedge-shaped wettability pattern with certain wedge angle and certain wide side width, when the narrow side width is no smaller than a critical value, the long-distance SDPT was achieved. Besides the horizontal and straight serial-wedge-shaped wettability pattern, bubbles transportation on the complicated and curved serial-wedge-shaped wettability patterns could also be realized. In addition, we developed a universal method composed of electrochemical etching and laser etching to fabricate the serial-wedge-shaped wettability pattern on various engineering metal materials including Al, Mg alloy, Ti alloy, and Zn. Based on the aforementioned results, it is hopeful that the serial-wedge-shaped wettability pattern can be fabricated on the inner wall surface of the pipelines and can effectively collect, transport, and eliminate gas bubbles in fluid transportation pipes.

2 Experiment Section

2.1 Fabrication of the serial-wedge-shaped wettability pattern

The aluminium plate (Al, purity > 99%) was first electrochemically etched in 0.1 mol/L aqueous sodium chloride (NaCl) solution at 500 mA/cm^2 current density for 10 min to obtain micrometer-scale rough structures. Thereinto, the anode-cathode distance was set at 30 mm. After electrochemical etching, the Al surface was shown to be superhydrophilic. Then, the superhydrophilic Al plate was immersed in the 1 wt.% solution of Fluoroalkylsilane (FAS, $C_8F_{13}H_4Si(OCH_2CH_3)_3$, Degussa Co., Germany) in ethanol for 1 h, which deposited the FAS layer on the micrometer-scale rough structures and lowered the surface energy. After FAS modification, the Al surface was superhydrophobic. Finally, the exterior surrounding region of the superhydrophobic Al surface was etched by a fiber laser marking system (SK-CX30, Shanghai Sanke Laser Technology Co., China) at 20 W power, 20 kHz frequency, 1064 nm central wavelength, 50 μm shift of scanning lines, and 2000 mm/s traverse speed to remove FAS layer. The laser scanning was performed line-by-line in the horizontal direction. After irradiation, the laser-etched region was transferred into superhydrophilic from superhydrophobic. Since the moving path of the laser can be designed and controlled by computer, the serial-wedge-shaped wettability pattern with adjustable size composed of the exterior surrounding superhydrophilic region with water contact angle of 0° and inside interior superhydrophobic region with water contact angle of 159.0±2.3° was obtained. The laser etching processes were inspired by Hwang *et al*.[34] and Megaridis *et al*.[35, 36]

2.2 Sample characterization

The micro-morphologies of the samples were characterized using a scanning electron microscope (SEM, JSM-6360LV, Japan). The crystal structures were characterized using an X-ray diffractometer (XRD, Empyrean, Holland). The X-ray source was a Cu Kα radiation (k = 0.15418 nm), and was operated within the 5-100° range and at a scanning rate of 2θ=0.026 °/min. The chemical compositions were characterized using a Fourier-transform infrared spectrophotometer (FTIR, JACSCO, Japan). Surface roughness value, Ra, was investigated using a surface profiler (Zygo, NV5000 5022S, USA). The contact angles (CA) of water in air and gas bubbles underwater were measured according to the sessile-drop method using an optical contact angle meter (Krüss, DSA100, Germany). The adhesive force between gas bubbles and the sample surfaces were measured using a high-sensitivity microelectromechanical balance system (Metter A60, Germany). The volumes of water droplets and gas bubbles used in the measurement of contact angles, sliding angles, advancing contact angles, receding contact angles and adhesive force were 5 μL and 2 μL, respectively. The transportation processes of subaqueous gas bubbles with volume of 40 μL on the samples were recorded using a high-speed camera (1000 frame/s, DSC-RX10 III, Sony, Japan) at ambient temperature. Air bubbles were used as gas bubbles and pure nitrogen jet (25 mL/min) were used as gas jet in the experiments.

3 Results and discussion

We developed a facile electrochemical etching and laser etching method to fabricate the serial-wedge-shaped wettability pattern composed of the exterior surrounding superhydrophilic region and inside interior superhydrophobic region. Several single-wedge-shaped patterns were connected end to end (a front triangle and several rear trapezoids with same size and shape), showing that the terminal size has no relationship with the length of the whole pattern. The schematics for the fabrication processes used are shown in Fig. 1(a). The digital photo and schematic of the sample are shown in Fig. 1(b) and Fig. S1. After electrochemical etching and FAS modification, the Al plate was superhydrophobic. The micro morphology shows that the electrochemically etched and FAS-modified Al surface had micrometer-scale rough structures composed of the rectangular-shaped plateaus and step-like structures with sizes in the range of 1 μm to 5 μm, as shown in Fig. 1(c). Then, the exterior surrounding region of the superhydrophobic Al surface was etched by laser. The size and shape of the laser-etched region was designed and controlled by computer. The laser-etched region was superhydrophilic. The SEM images show that the whole micro morphology after laser etching was changed and was composed of micrometer-scale pores of size 40 μm with protrusions of size 20 μm, as shown in Fig. 1(d) and Fig. S2. The surfaces of the pore walls and protrusions were also very rough and composed of particles with size of 100 nm to 4 μm. The XRD

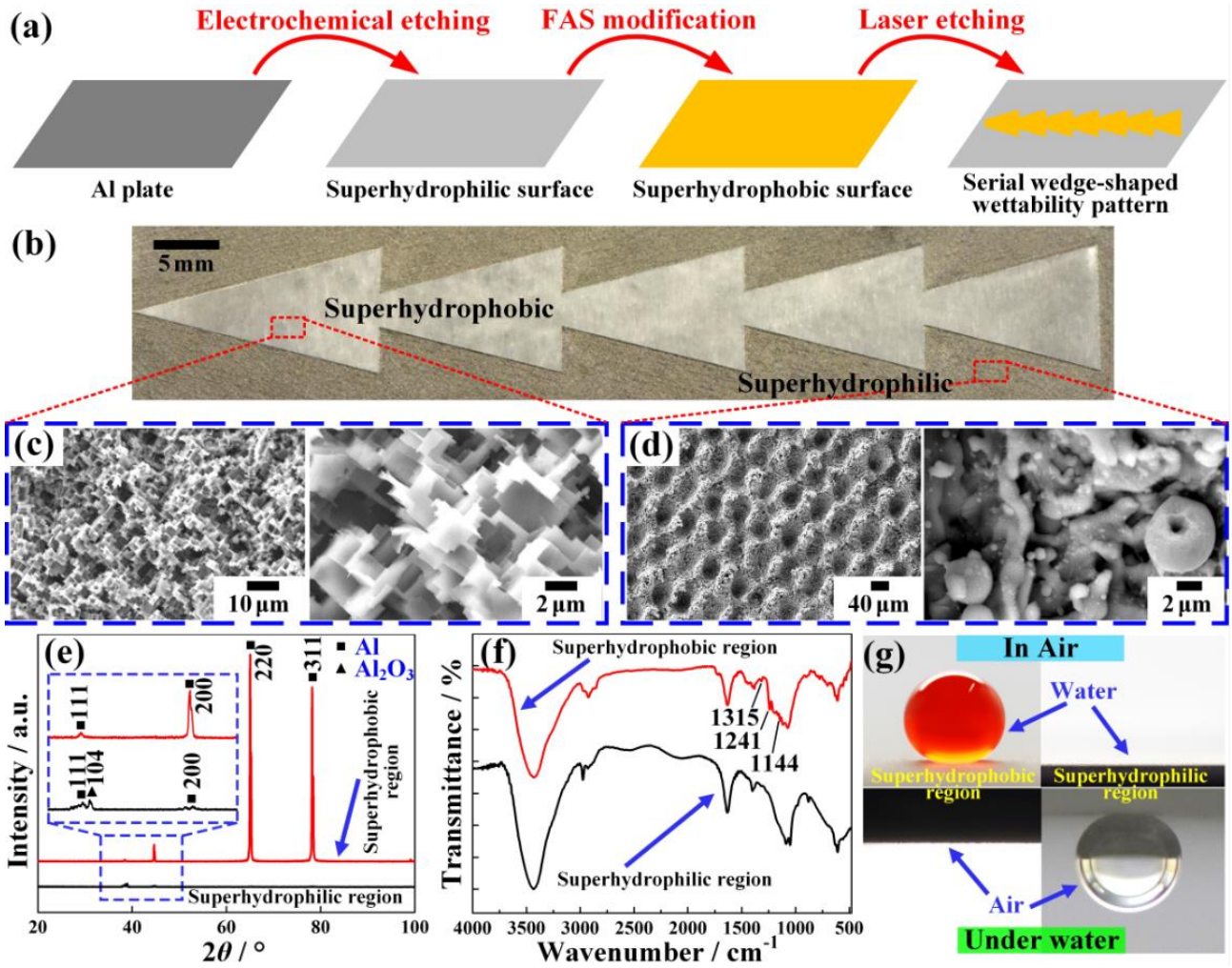

Fig. 1 The schematics of the fabrication processes and surface morphology, chemical composition, and wettability of the serial-wedge-shaped wettability pattern. (a) The schematics of the fabrication processes. (b) The digital photo of the serial-wedge-shaped wettability pattern with the exterior surrounding subaqueous superaerophobic region and inside interior subaqueous superaerophilic region. Several single-wedge-shaped patterns were connected end to end (a front triangle and several rear trapezoids with same size and shape), showing that the terminal size has no relationship with the length of the whole pattern. (c) SEM images of superhydrophobic region with different magnifications. (d) SEM images of superhydrophilic region with different magnifications. (e) XRD patterns of superhydrophilic region and superhydrophobic region. The diffraction peaks assigned to Al or Al_2O_3 are referenced to JCPDS Card No. 04-0787 and No. 35-0121, respectively. (f) FTIR spectra of superhydrophilic region and superhydrophobic region. The absorption bands at around 1315, 1241, and 1144 cm^{-1} are assigned to the C–F stretching vibration of the–CF_3 and –CF_2– groups of the FAS molecules and appeared on the electrochemically etched and FAS-modified Al surface but not appeared on the laser-etched Al surface. (g) The water droplet with volume of 5 μL and subaqueous gas bubble with volume of 2 μL on the superhydrophilic region and superhydrophobic region.

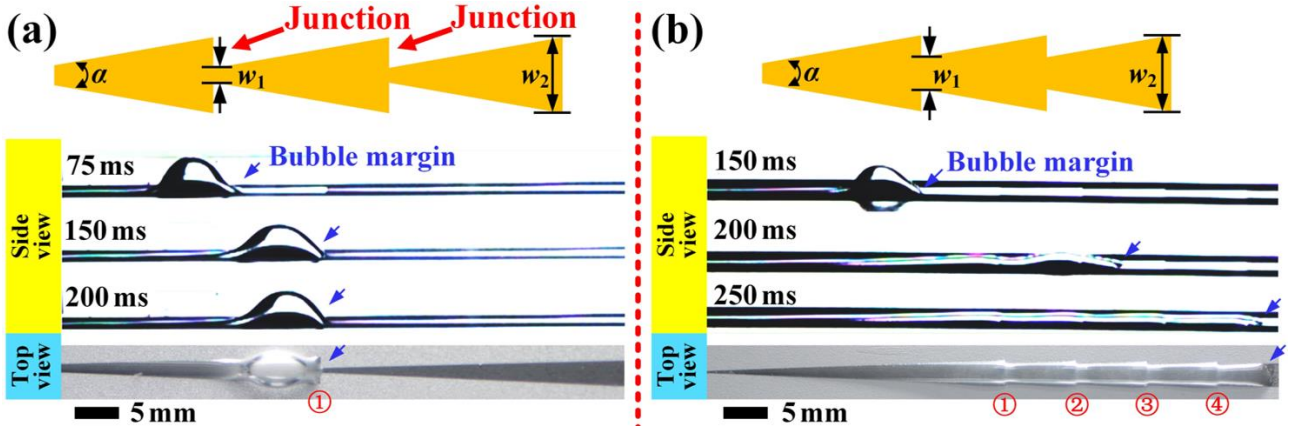

Fig. 2 The transportation processes of a subaqueous gas bubble with volume of 40 μL on the serial-wedge-shaped wettability pattern. (a) For α=4°, w_1=0.4 mm, and w_2=2 mm, the gas bubble stopped and stayed at the first junction, meaning a failed continuous transportation. (b) For α=4°, w_1=1.6 mm, and w_2=2 mm, the gas bubble crossed the junction and the continuous SDPT was realized. The arrow points to the margin of the gas bubble. The number ①②③④ represent the number of the junction counting from the left of the initial position.

pattern indicates that the main composition of the micro structures on the electrochemically etched and FAS-modified Al surface were Al, while the main composition of the micro structures on the laser-etched surface were Al and Al_2O_3, as shown in Fig. 1(e). The Al_2O_3 was resulted from the melt and re-solidification of Al in the laser etching processes. In the FTIR spectra, the absorption bands assigned to the C–F stretching vibration of the $–CF_3$ and $–CF_2$ groups of the FAS molecules were detected on the electrochemically etched and FAS-modified Al surface but were not detected on the laser-etched Al surface, indicating that the FAS layer was removed by laser in the laser etching processes, as shown in Fig. 1(f). The generation of the new rough structures and the removal of the FAS with low surface energy in the laser etching processes resulted in the transition of wettability from superhydrophobicity to superhydrophilicity. The water droplet in air showed a globular shape with CA of 159.0±2.3° (details in Table S1) on the superhydrophobic region but spread completely with CA of 0° on the superhydrophilic region, as shown in Fig. 1(g) and Video S1. When the sample was immersed in water, the wettability situation was immersed in water, the wettability situation was changed. The gas bubble under water spread completely with CA of 0° on the superhydrophobic region (also can be called as "subaqueous superaerophilicity") but showed a globular shape with CA of 155.0±2.8° on the superhydrophilic region (also can be called as "subaqueous superaerophobicity"). Then, the serial-wedge-shaped wettability pattern with the exterior surrounding subaqueous superaerophobic region and inside interior subaqueous superaerophilic region was obtained. The adhesive force of gas bubbles on the subaqueous superaerophobic region was as low as 3.5±1.2 μN (details in Fig. S3). Such a low adhesive force on the exterior surrounding region will help to make gas bubbles easier to transport only on the inside interior subaqueous superaerophilic region.

We next tested if the serial-wedge-shaped wettability pattern can realize the continuous SDPT of subaqueous gas bubbles. The serial-wedge-shaped wettability patterns with a wedge angle α=4° and wide side width w_2=2 mm and different narrow side width w_1 were horizontally placed under water. A gas bubble with volume of 40 μL was placed on the horizontal samples by a high precision syringe. Once contacted with the narrow side of the serial-wedge-shaped wettability pattern, the gas bubble was immediately captured and spontaneously and directionally transported toward the wide side. However, we found that the narrow side width w_1 had a large influence on the transportation distance of subaqueous gas bubbles. For w_1=0.4 mm, the transportation distance was only that of the first wedge with length of 22.91 mm then the gas bubble stopped and stayed at the first junction, meaning that gas bubble cannot be transported continuously, as shown in Fig. 2(a) and Video S2. Bubble margin in Figure 2 shows the position of the front of the gas bubble. However, for w_1=1.6 mm, it was easy for the gas bubble to cross the junction and the continuous SDPT was achieved, as shown in Fig. 2(b). This experiment indicates that for the serial-wedge-shaped wettability pattern with certain wedge angle and certain wide side width, if the narrow side width is suitable, the long-distance SDPT of subaqueous gas bubbles can be achieved.

We then studied the relationship between the narrow side width and transportation distance and transportation velocity of subaqueous gas bubbles on the serial-wedge-shaped wettability pattern with certain wedge angle and certain wide side width. For α=4°, when (w_1, w_2) were (0.4 mm, 1 mm), (0.6 mm, 1mm), (0.8 mm, 2 mm), and (0.6 mm, 3 mm) respectively, gas bubbles transported fluently first with an increasing distance and velocity, but suddenly stopped at the first junction with the transportation distance of about 8.67 mm for w_2=1 mm, 22.91 mm for w_2=2 mm, and 37.22 mm for w_2=3 mm, as shown in Figs. 3(a) to 3(c). When (w_1, w_2) were (0.8 mm, 1 mm), (1 mm, 2 mm), (1.2 mm, 2 mm), (0.8 mm, 3 mm), and (1 mm, 3 mm), gas bubbles also transported fluently first with an increasing distance and velocity before arriving at the first junction but then crossed the junction fluently and realized the continuous SDPT. Additionally, to evaluate the effect of surface roughness on the transportation behavior, we transported gas bubbles on three serial-wedge-shaped wettability patterns with the same geometric parameters (α=4°, w_1=1.2 mm, w_2=2 mm) but different surface roughness (Ra), as shown in Fig. S4. We found that the surface roughness almost had no effect on the transportation behavior of gas bubbles. The aforementioned results indicate that for certain α and w_2, there is a critical w_{1c} such that when the narrow side width is no smaller than that critical w_{1c}, the continuous SDPT can be realized. For α=4°, the serial-wedge-shaped

wettability pattern with w_2= 1 mm & $w_1 \geq$ 0.8 mm, or w_2= 2mm & $w_1 \geq$ 1.0 mm, or w_2= 3 mm

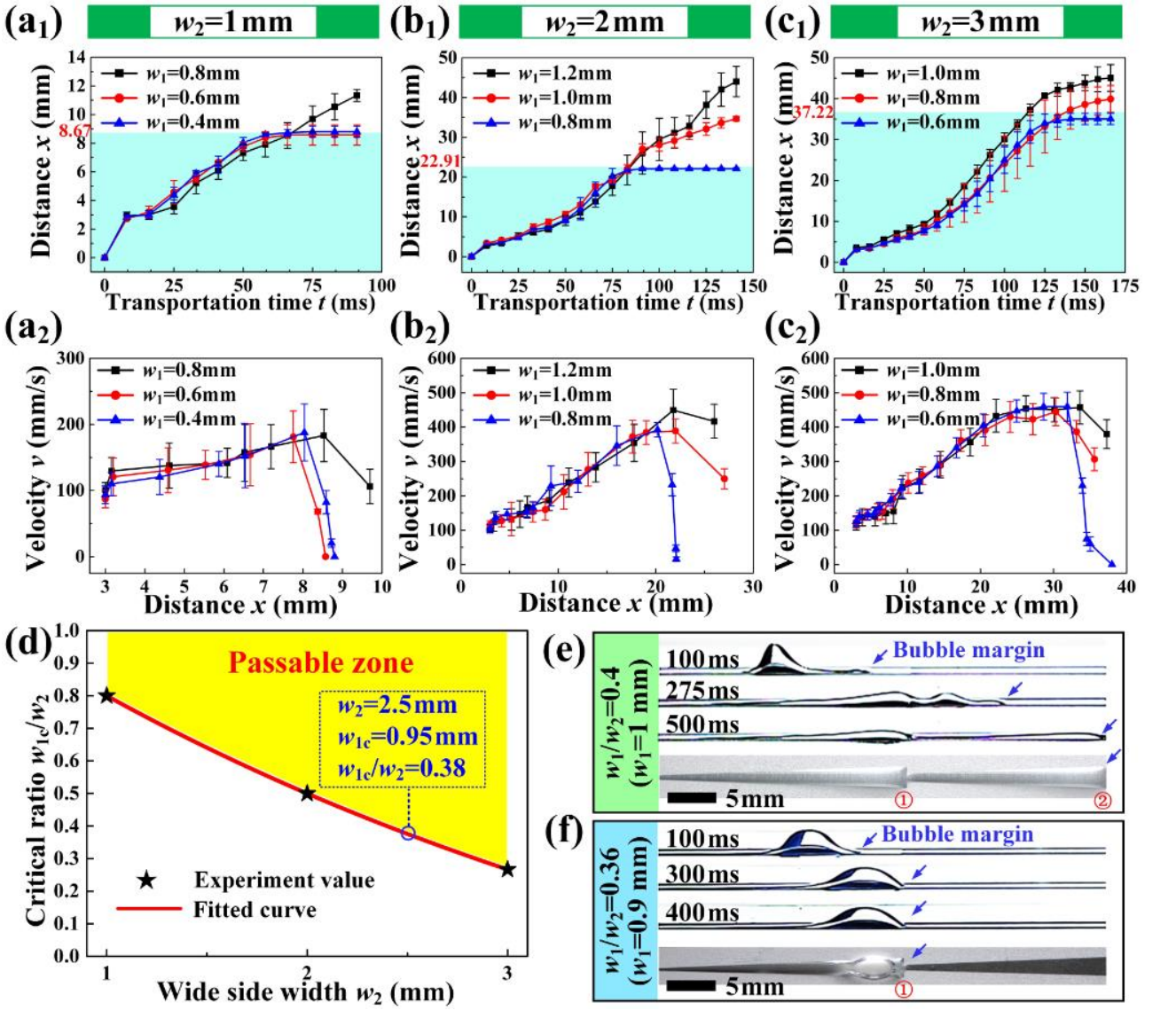

Fig. 3 The effect of the narrow side width of the serial-wedge-shaped wettability pattern with certain wedge angle and certain wide side width on the transportation behavior of a subaqueous gas bubble with volume of 40 μL. The wedge angle α=4°. The relationship between the transportation distance and transportation time at different w_1 with w_2=1 mm (a_1), w_2=2 mm (b_1), and w_2=3 mm (c_1). The relationship between the transportation velocity and transportation distance at different w_1 with w_2=1 mm (a_2), w_2=2 mm (b_2), and w_2=3 mm (c_2). (d) The relationship between w_{1c}/w_2 and w_2 at α=4°. The critical w_{1c} means the smallest narrow side width that can realize the continuous SDPT for a certain w_2. (e) The serial-wedge-shaped wettability pattern with w_1=1 mm and w_2=2.5 mm can realize the continuous SDPT. (f) The serial-wedge-shaped wettability pattern with w_1=0.9 mm and w_2=2.5 mm cannot realize the continuous SDPT. The arrow points to the margin of the gas bubble. The number ①② represent the number of the junction counting from the left of the initial position.

& $w_1 \geq$ 0.8 mm can realize the continuous SDPT. The relationship between (the critical w_{1c})/w_2 and w_2 at α=4° is shown in Fig. 3(d) and a corresponding curve-fit is as follows,

$$\frac{w_{1c}}{w_2} = -0.55 + 1.73e^{-0.25w_2} \qquad (1 \leq w_2 \leq 3) \qquad (1)$$

Then the critical w_{1c} for a certain w_2 is given by

$$w_{1c} = w_2(-0.55 + 1.73e^{-0.25w_2}) \quad (1 \leq w_2 \leq 3) \qquad (2)$$

We performed the following experiments to verify Equations (1) and (2). For the serial-wedge-shaped wettability pattern with α=4°and w_2=2.5 mm, the critical w_{1c} according to the aforementioned Equations is about 0.95 mm. Then, we fabricated the samples with w_1=1 mm and 0.9 mm and found that the gas bubble on the serial-wedge-shaped wettability pattern with w_2=2.5 mm and w_1=1 mm can cross the junction fluently and realize the continuous SDPT (Fig. 3(e)), while for the pattern with w_2=2.5 mm and w_1=0.9 mm, the gas bubble stopped at the first junction (Fig. 3(f)). The fitting result agreed well with the experimental ones. Using the similar method, we also obtained the relationship between(the critical w_{1c})/w_2 and w_2 at α=2°, 3°, and 5°, as shown in Fig. S5.

We then theoretically studied why the narrow side width w_1 plays a key role on the transportation behavior of subaqueous gas bubbles on the serial-wedge-shaped wettability pattern with certain wedge

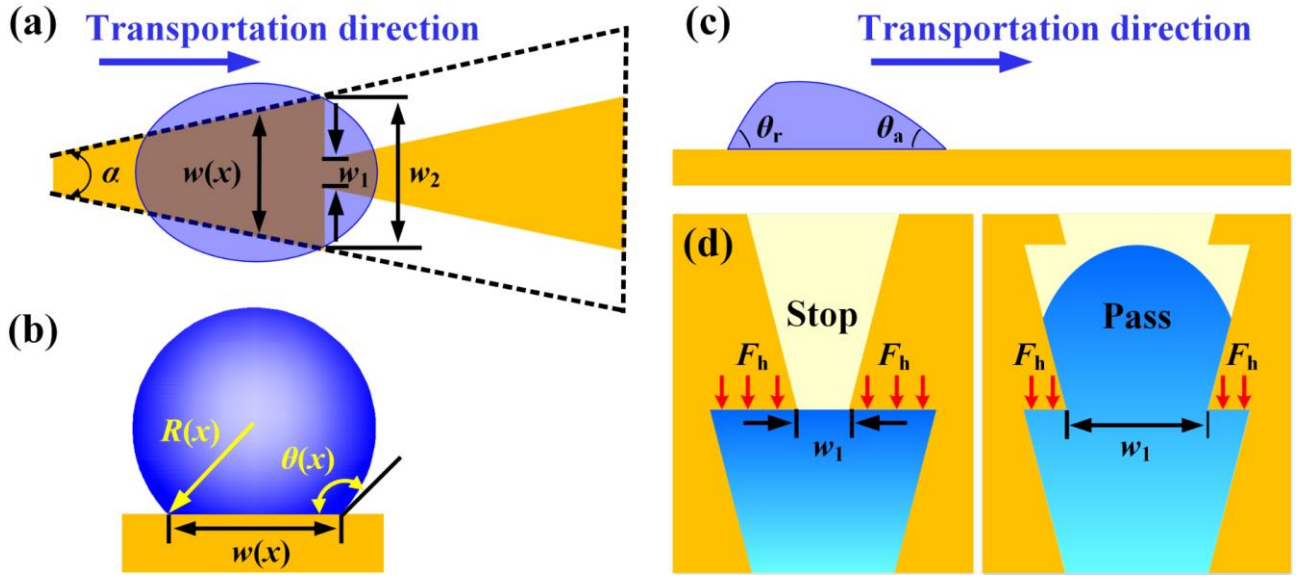

Fig. 4 Schematic analysis of subaqueous gas bubbles on the serial-wedge-shaped wettability pattern. (a) Compared with single-wedge-shaped wettability pattern (the dotted area) showed the gas bubble suffers an additional hysteresis resistance force at the junction on the serial-wedge-shaped wettability pattern. (b) Schematic of the cross section area of the gas bubble in the transportation direction. (c) Schematic of the side view of bubble transportation. (d) Small w_1 means large F_h and hinders the transportation of air bubbles; while big w_1 means smaller F_h and gas bubbles cross the junction fluently.

angle α and certain wide side width w_2. The schematic of the transportation processes is shown in Fig. 4. The main driving force F_d for the gas bubble along the superaerophilic serial-wedge-shaped track is the unbalanced surface tension force originated from Laplace pressure difference between its front and back. The Laplace pressure $p(x)$ at any transportation distance x is $\sim \gamma/R(x)$, where γ is the interfacial tension for gas-water and the local curvature of the gas bubble on the superaerophilic track $R(x) \approx w(x)/2\sin\theta(x)$; $w(x)$ denotes the superaerophilic track width and $\theta(x)$ is the apparent contact angle of the gas bubble on the superaerophilic track and along the two straight edges, as shown in Fig. 4(a) and 4(b). The net axial Laplace pressure gradient $dp(x)/dx$ in the gas bubble can be estimated as, [11]

$$\frac{dp(x)}{dx} \sim \frac{d[\gamma / R(x)]}{dx} \sim \frac{d[2\gamma \sin\theta(x) / w(x)]}{dx} \quad (3)$$

Then, the main driving force

$$F_d \sim \int \frac{d[2\gamma \sin\theta(x) / w(x)]}{d(x)} S(x)\, dx \quad (4)$$

Where $S(x)$ denotes the cross section area of the gas bubble in the transportation direction. The main drag force for the gas bubble along the superaerophilic serial-wedge-shaped track is the pressure difference resistance force F_p and hysteresis resistance force F_h. F_p exist in the whole transportation process and can be demonstrated as follows,

$$F_p = \frac{1}{2} C \rho v(x)^2 S(x) \quad (5)$$

where C is the drag coefficient of water, ρ is the density of water, $v(x)$ is the transportation velocity of the gas bubble along the superaerophilic serial-wedge-shaped track at any transportation distance x. F_h mainly exists at the junction and can be expressed as the *Furmidge* equation[37],

$$F_h = \gamma(w_2 - w_1)(\cos\theta_a - \cos\theta_r) \quad (6)$$

where θ_r and θ_a denote the receding and advancing contact angles of the gas bubble at the junction as shown in Figure 4(c), respectively. Then, according to Equations (4), (5), and (6), the resultant force (F_r) acting on the gas bubble at the junction can be estimated as $F_r = F_d - F_p - F_h$. For the serial-wedge-shaped wettability pattern with certain wedge angle α and wide side width w_2 and a gas bubble with certain volume, F_d and F_p were certain at the first junction while F_h was seriously affected by w_1. The F_h decreases while the F_r increases with larger w_1. Smaller w_1 will produce larger F_h and hinder the transportation of the gas bubble, as shown in Fig. 4(d). The analysis result is in good agreement with the experimental result shown in Figure 3(a_1, b_1, c_1) that bubbles can cross the junction fluently on the pattern with larger w_1 but stopped at the junction on the pattern with smaller w_1.

In order to further certify the importance of the wedge-shape, we also fabricated a rectangle wettability pattern with a constant width of 2 mm composed of the exterior surrounding subaqueous superaerophobic region and inside interior subaqueous superaerophilic region on Al substrate by the developed electrochemical etching and laser etching method. Once contacted with the left side of the rectangle wettability pattern, the gas bubble with volume of 40 μL was immediately captured. However, owing to the lack of driving force originated from geometric gradient, the gas bubble was stopped and could not be transported on the rectangle wettability pattern, as shown in Fig. S6 and Video S3.

To further prove the long-distance SDPT ability, a gas bubble with volume of 40 μL was put on a horizontal and straight serial-wedge-

shaped wettability pattern with α=4°, w_1=1.6 mm, w_2=2 mm and 10 junctions. The gas bubble was captured and spread immediately on the superaerophilic serial-wedge-shaped track and spontaneously and directionally transported toward the terminal side. It was easy for the gas bubble to cross 10 junctions and achieve a transportation distance of 80 mm, as shown in Fig. 5(a), Video S4, and Video S5. Besides the

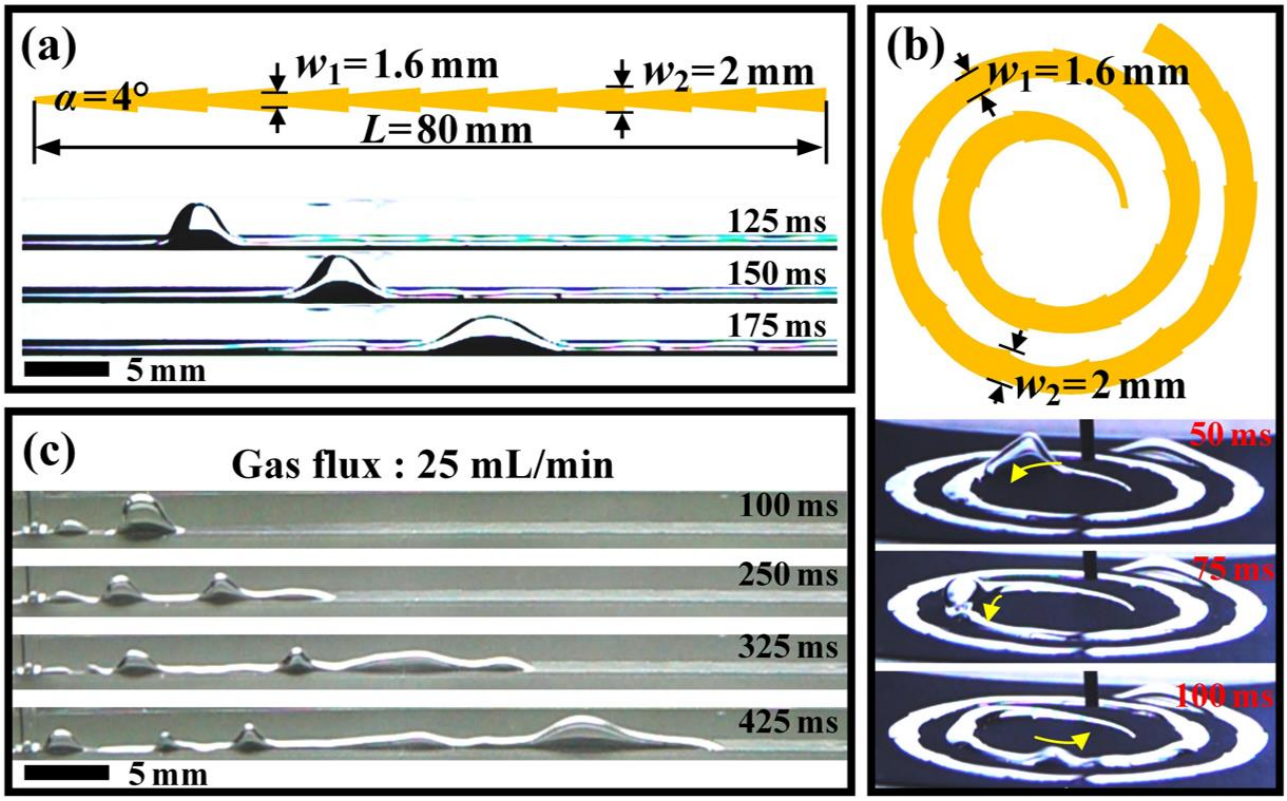

Fig. 5 The long-distance SDPT processes of a gas bubble and gas jet on the serial-wedge-shaped wettability pattern. (a) The long-distance SDPT processes of a gas bubble with volume of 40 μL on a straight serial-wedge-shaped wettability pattern with α=4°, w_1=1.6 mm, and w_2=2 mm. (b) The long-distance SDPT processes of a gas bubble with volume of 40 μL on a spiral-shaped serial-wedge-shaped wettability pattern with α=4°, w_1=1.6 mm, and w_2=2 mm. (c) The long-distance SDPT processes of gas jet with flux of 25 mL/min on the serial-wedge-shaped wettability pattern with α=4°, w_1=2.6 mm, and w_2=3 mm.

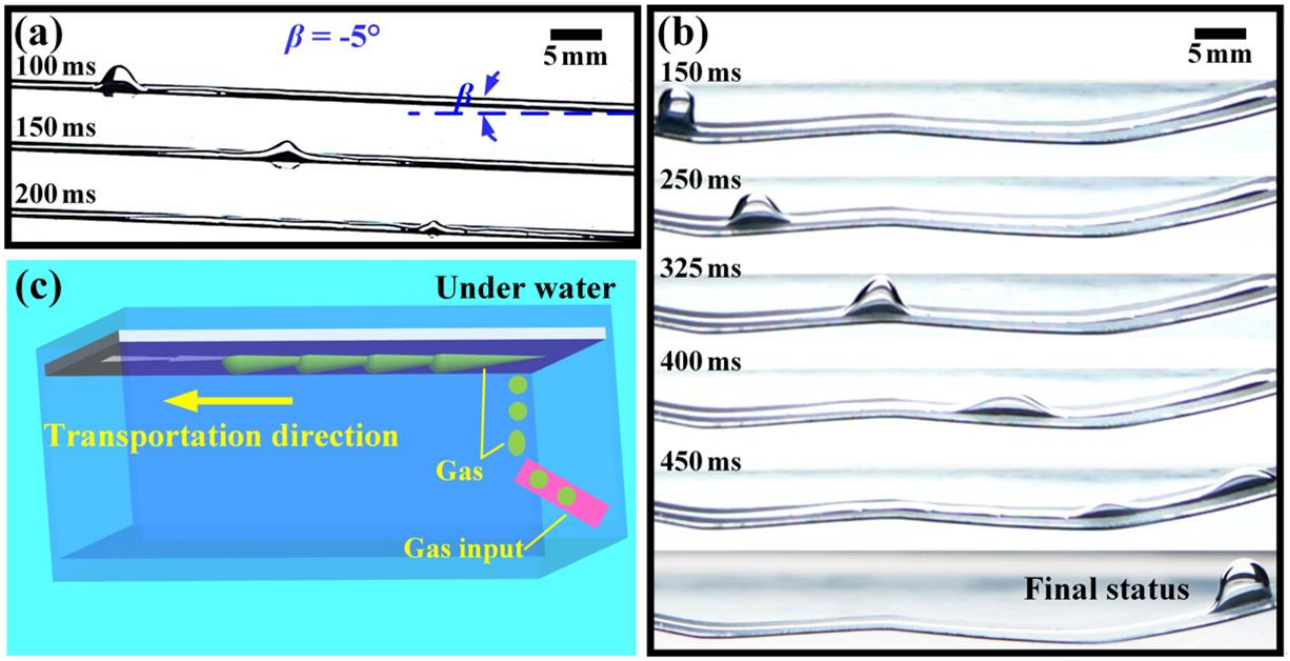

Fig. 6 The transportation behavior of subaqueous gas bubbles on the serial-wedge-shaped wettability pattern in the complex condition. (a) The downhill SDPT processes of a gas bubble with volume of 40 μL on a serial-wedge-shaped wettability pattern with α=4°, w_1=1.6 mm, and w_2=2

mm. The titled angle β for the sample is -5°. (b) The SDPT processes of a gas bubble with volume of 40 μL on a spatial wave-shaped serial-wedge-shaped wettability pattern with α=4°, w_1=1.6 mm, and w_2=2 mm. (c) The SDPT processes of gas bubbles on the serial-wedge-shaped wettability pattern (α=4°, w_1=1.6 mm, and w_2=2 mm) which was fixed on the top wall surface of a square tube with face down.

horizontal and straight serial-wedge-shaped wettability pattern, the other complicated and curved serial-wedge-shaped wettability pattern can also realize the long-distance SDPT, for example the horizontal and spiral-shaped pattern as shown in Fig. 5(b) and Video S6. The long-distance SDPT ability of the serial-wedge-shaped wettability pattern can also be proved by the transportation of gas jet with high flux. Fig. 5(c) and Video S7 show the transportation processes of gas jet with a flux of 25 mL/min. Although gas bubbles flowed out from the glass tube continuously with a high flux, all gas bubbles were captured by the serial-wedge-shaped wettability pattern with α=4°, w_1=2.6 mm, and w_2=3 mm. With the continuous capture of gas bubbles, a gas film with a gradually increased thickness in approaching to the terminal side of the pattern was generated. Finally, all of the captured gas bubbles were developed into a big gas bubble at the terminal side of the pattern. The buoyancy force of the big gas bubble at the terminal side increased with the bubble's volume and finally at the largest sizes made the gas bubble detach from the pattern.

The serial-wedge-shaped wettability pattern can also realize anti-buoyancy SDPT. As shown in Fig. 6(a) and Video S8, a gas bubble with volume of 40 μL was transported downhill fluently along the superaerophilic serial-wedge-shaped track with a titled angle of -5°. This anti-buoyancy transportation ability indicates that the long-distance SDPT of subaqueous gas bubble on the serial-wedge-shaped wettability pattern can be realized in the complex condition, for example the transportation on the spatial wave-shaped samples. Fig. 6(b) and Video S9 show the transportation processes of a gas bubble with volume of 40 μL on the spatial wave-shaped pattern with a length of 80 mm. Although the buoyancy was the resistant force on particular sections on the spatial wave-shaped pattern, the gas bubble overcame the resistance of buoyancy and successfully transported from the initial side to the terminal side.

For fluid transportation pipes, gas bubbles easily touch the top wall surface of the pipes because of buoyancy. In order to simulate the aforementioned situation, we put the serial-wedge-shaped wettability pattern with face down on the top wall surface of a square tube (Fig. S7). Subaqueous gas bubbles that touched the pattern were also immediately captured and transported, as shown in Fig. 6(c) and Video S10, further indicating the practicality of the serial-wedge-shaped wettability pattern on collecting, transporting and eliminating subaqueous gas bubbles in fluid transportation pipes.

Since the serial-wedge-shaped wettability pattern with the exterior surrounding subaqueous superaerophobic region and inside interior subaqueous superaerophilic region can realize the long-distance SDPT of subaqueous gas bubbles, we wondered if this phenomenon can be extended to the transportation of organic liquid under water and the transportation of water in air. We found that the serial-wedge-shaped wettability pattern shown in Fig. 5(a) could spontaneously, directionally, continuously, and over long-distance transport dichloromethane under water, as shown in Video S11. For water in air, we fabricated a serial-wedge-shaped wettability pattern with an exterior surrounding superhydrophobic region and inside interior superhydrophilic region with α=4°, w_1=1.6 mm, w_2=2 mm, 10 junctions and 80 mm length and we found that this serial-wedge-shaped wettability pattern could very easily realize the long-distance SDPT of a 20 μL water droplet accompanied by crossing all the junctions, as shown in Video S12. The aforementioned findings increase the range of the applications of the serial-wedge-shaped wettability pattern.

In 2016 and 2018, Megaridis et al. used a method composed of hydrochloric acid (HCl) etching, boiling water immersion and laser etching to fabricate the single-wedge-shaped wettability pattern on Al substrate with an exterior surrounding superhydrophobic region and inside interior superhydrophilic region.[35, 36] However, their method seems only effective for Al materials. A universal method to fabricate the serial-wedge-shaped wettability pattern on various engineering metal materials will greatly promote its practical application. Fortunately, the method developed by us, which is composed of electrochemical etching and laser etching, is universal. As shown in Fig. S8 and Video S13, the serial-wedge-shaped wettability pattern was easily fabricated on Mg alloy materials, Ti alloy materials, and Zn materials, respectively.

4 Conclusions

In summary, we developed a serial-wedge-shaped wettability pattern with the exterior surrounding subaqueous superaerophobic region and inside interior subaqueous superaerophilic region to realize the long-distance, spontaneous, directional, and pumpless transportation (SDPT) of subaqueous gas bubbles. We carefully observed the transportation behaviour of gas bubbles on the serial-wedge-shaped wettability pattern and found that whether gas bubbles could cross the junction fluently would directly determine whether long-distance SDPT could be achieved. We then systemically studied the influence of the narrow side width on the transportation behaviour of subaqueous gas bubbles on the serial-wedge-shaped wettability pattern with certain wedge angle and certain wide side width and got an equation and a fitting curve for the relationship between the critical narrow side width and the wide side width at different wedge angle. According to the equation and fitting curve, when the narrow side width is no smaller than that critical value, the long-distance SDPT could be achieved. Subaqueous gas bubbles can not only be spontaneously and directionally transported on the horizontal and straight pattern, but also can easily be transported on the horizontal and spiral-shaped pattern or even anti-buoyancy transported on the spatial tilted and wave-shaped pattern. In addition, we developed a universal method composed of electrochemical etching and laser etching to fabricate the serial-wedge-shaped wettability pattern on various engineering metal materials including Al, Mg alloy, Ti alloy, and Zn. The realization of the long-distance SDPT of subaqueous gas bubbles and the fabrication of the long-distance SDPT surface on various engineering metal materials make it promising to effectively collect, transport, and eliminate gas bubbles in fluid transportation pipes.

Conflicts of interest

There are no conflicts to declare.

Acknowledgement

This work was financially supported by National Natural Science Foundation of China (NSFC, 51605078, 21774051), the Science Fund for Creative Research Groups of NSFC (51621064), Young

Elite Scientists Sponsorship Program by CAST (YESS, 2017QNRC001), Aviation Science Fund (2017ZE63012), and the Fundamental Research Funds for the Central Universities (DUT17JC25). Y.L. acknowledges the support from EPSRC project EP/N024915/1.

References

1 Y. Lu, S. Sathasivam, J. Song, C. R. Crick, C. J. Carmalt and I. P. Parkin, *Science*, 2015, **347**, 1132.
2 X. Deng, L. Mammen, H. J. Butt and D. Vollmer, *Science*, 2012, **335**, 67.
3 X. Tian, T. Verho and R. H. Ras, *Science*, 2016, **352**, 142.
4 J. Yong, F. Chen, Q. Yang, J. Huo and X. Hou, *Chem. Soc. Rev.*, 2017, **46**, 4168.
5 Z. Zhu, S. Zheng, S. Peng, Y. Zhao and Y. Tian, *Adv. Mater.*, 2017, **29**, 1703120.
6 Y. Peng, X. Jin, Y. Zheng, D. Han, K. Liu and L. Jiang, *Adv. Mater.*, 2017, **29**, 1703009.
7 T. M. Schutzius, S. Jung, T. Maitra, G. Graeber, M. Köhme and D. Poulikakos, *Nature*, 2015, **527**, 82.
8 F. Xiao, S. Yuan, B. Liang, G. Li, S. O. Pehkonen and T. Zhang, *J. Mater. Chem. A*, 2015, **3**, 4374.
9 J. Ge, L. Shi, Y. Wang, H. Zhao, H. Yao, Y. Zhu, Y. Zhang, H. Zhu, H. Wu and S. Yu, *Nat. Nanotechnol.*, 2017, **12**, 434.
10 H. Hu, J. Wen, L. Bao, L. Jia, D. Song, B. Song, G. Pan, D. Scaraggi, D. Dini, Q. Xue and F. Zhou, *Sci. Adv.*, 2017, **3**, e1603288.
11 A. Ghosh, R. Ganguly, T. M. Schutzius and C. M. Megaridis, *Lab Chip*, 2014, **14**, 1538.
12 K. Li, J. Ju, Z. Xue, J. Ma, L. Feng, S. Gao and L. Jiang, *Nat. Commun.*, 2013, **4**, 2276.
13 V. Hejazi and M. Nosonovsky, *Langmuir*, 2012, **28**, 2173.
14 S. Gao, J. Sun, P. Liu, F. Zhang, W. Zhang, S. Yuan, J. Li and J. Jin, *Adv. Mater.*, 2016, **28**, 5307.
15 V. Hejazi, A. E. Nyong, P. K. Rohatgi and M. Nosonovsky, *Adv. Mater.*, 2012, **24**, 5963.
16 C. Yu, P. Zhang, J. Wang and L. Jiang, *Adv. Mater.*, 2017, **29**, 1703053.
17 Z. Zhu, S. Zheng, S. Peng, Y. Zhao and Y. Tian, *Adv. Mater.*, 2017, **29**, 1703120.
18 Z. Lu, W. Zhu, X. Yu, H. Zhang, Y. Li, X. Sun, X. Wang, H. Wang, J. Wang, J. Luo, X. Lei and L. Jiang, *Adv. Mater.*, 2014, **26**, 2683.
19 Z. Lu, M. Sun, T. Xu, Y. Li, W. Xu, Z. Chang, Y. Ding, X. Sun and L. Jiang, *Adv. Mater.*, 2015, **27**, 2361.
20 Y. Li, H. Zhang, T. Xu, Z. Lu, X. Wu, P. Wan, X. Sun and L. Jiang, *Adv. Funct. Mater.*, 2015, **25**, 1737.
21 J. He, B. Hu and Y. Zhao, *Adv. Funct. Mater.*, 2016, **26**, 5998.
22 Q. Zhang, P. Li, D. Zhou, Z. Chang, Y. Kuang, and X. Sun, *Small*, 2017, **13**, 170164841.
23 Z. Lu, Y. Li, X. Lei, J. Liu and X. Sun, *Mater. Horiz.*, 2015, **2**, 294.
24 P. Zhang, J. Zhang, Z. Xue, J. Wang and L. Jiang, *Mater. Horiz.*, 2017, **4**, 665.
25 J. Han, J. Zhang and J. W. Carey, *Int. J. Greenh. Gas. Con.*, 2011, **5**, 1680.
26 A. Samimi, *Int. J. Innov. and Appl. Stud.*, 2012, **1**, 165.
27 X. Chen, Y. Wu, B. Su, J. Wang, Y. Song and L. Jiang, *Adv. Mater.*, 2012, **24**, 5884.
28 C. Yu, X. Zhu, M. Cao, C. Yu, K. Li and L. Jiang, *J. Mater. Chem. A*, 2016, **4**, 16865.
29 C. Yu, X. Zhu, K. Li, M. Cao and L. Jiang, *Adv. Funct. Mater.*, 2017, **27**, 170160529.
30 C. Yu, M. Cao, Z. Dong, J. Wang, K. Li and L. Jiang, *Adv. Funct. Mater.*, 2016, **26**, 3236.
31 X. Xue, C. Yu, J. Wang and L. Jiang, *ACS Nano*, 2016, **10**, 10887.
32 H. Ma, M. Cao, C. Zhang, Z. Bei, K. Li, C. Yu and L. Jiang, *Adv. Funct. Mater.*, 2018, **28**, 17050917.
33 C. Zhang, B. Zhang, H. Ma, Z. Li, X. Xiao, Y. Zhang, X. Cui, C. Yu, M. Cao and L. Jiang, *ACS Nano*, 2018, **12**, 2048.
34 C. Lee, H. Cho, D. Kim and W. Hwang, *Appl. Surf. Sci.*, 2014, **288**, 619.
35 T. P. Koukoravas, A. Ghosh, P. S. Mahapatra, R. Ganguly and C. M. Megaridis, *Int. J. Heat Mass Tran.*, 2016, **95**, 142.
36 U. Sen, S. Chatterjee, R. Ganguly, R. Dodge, L. Yu and C. M. Megaridis, *Langmuir*, 2018, **34**, 1899.
37 C. G. L. Furmidge, *J. Colloid Sci.*, 1962, **17**, 309.

